Mater. Res. Soc. Symp. Proc. Vol. 832 © 2005 Materials Research Society F5.4.1

Growth and Overgrowth of Ge/Si Quantum Dots: An Observation by Atomic Resolution HAADF-STEM Imaging

Dan Zhi[1], Paul A. Midgley[1], Rafal E. Dunin-Borkowski[1], Bruce A. Joyce[2], Don W. Pashley[3], Andrew L. Bleloch[4], and Peter J. Goodhew[5]
[1]Department of Materials Science and Metallurgy, University of Cambridge, Pembroke Street, Cambridge CB2 3QZ, UK
[2]Department of Physics, Imperial College, London SW7 2AZ, UK
[3]Department of Materials, Imperial College, London SW7 2AZ, UK
[4]UK SuperSTEM Laboratory, Daresbury, Cheshire WA4 4AD
[5]Department of Engineering, University of Liverpool, Liverpool L69 3GH, UK

ABSTRACT

The formation of self-assembled quantum dots (QD) is of increasing interest for applications in optical, nanoelectronic, biological and quantum computing systems. From the perspective of fabrication technology, there are great advantages if the whole device can be made using a single Si substrate. Furthermore, GeSi is a model semiconductor system for fundamental studies of growth and material properties. In practice, as the MBE growth of heterostructures is inherently a non-equilibrium process, the formation of self-assembled nanostructures is both complex and sensitive to growth and overgrowth conditions. The morphology, structure and composition of QDs can all change during growth. It is therefore crucial to understand their structures at different stages of growth at the atomic scale. Here, the characterization of QD growth using high-resolution high angle annular dark field (HAADF) scanning transmission electron microscopy (STEM) imaging is presented. Both the formation of uncapped QDs and the effect of the encapsulation are investigated, and the morphological and compositional evolution of the QDs and wetting layers are observed directly at the atomic scale for the first time. During encapsulation, the Ge content in the centres of the QD remains unchanged, despite significant intermixing, lateral spreading and a laterally inhomogeneous Ge distribution inside the Ge QD. The initial non-uniform wetting layer for the uncapped Ge QD becomes uniform after encapsulation, and a 3-monolayer-thick core with ~ 60% Ge content is formed in the 2 nm-thick wetting layer with an average Ge content of ~ 30%. The results were obtained by direct analysis of the Z-contrast STEM imaging without involving complex image simulations.

INTRODUCTION

The formation of self-organized Ge islands on Si has generated considerable interest in the field of semiconductors in recent years [1]. In contrast to InAs dots, Ge/Si islands normally have a larger size and a lower density, preventing them from acting as QDs in optoelectronic devices. Low temperature growth and vertical stacking of dot layers, which results in size ordering, are being used to solve these problems. It is necessary to introduce size ordering, since the size distribution of small Ge islands can be broad as a result of their instability [2]. In the Ge/Si material system, which has been used widely as a model system for understanding heteroepitaxy, QD formation is well established both experimentally [3, 4-7] and theoretically [8, 9, 10]. From an experimental viewpoint, scanning tunneling microscopy (STM), which is a powerful and very sensitive probe for surface analysis, has

been one of the key techniques used to resolve surface QD structure [1, 3]. Despite many theoretical studies and high-resolution STM observations, the evolution of QDs during encapsulation and overgrowth is still not understood. In most theoretical models of the epitaxial growth of QDs, and most experimental observations, a QD-on-wetting layer configuration is accepted. Strain-driven alloying or intermixing in both the QD and the wetting layer, and QD shape change after capping, have also been predicted or observed, but the detailed structures of the QD and the wetting layer after capping are not known. The knowledge of the morphology and the chemical composition of QDs used in active regions of devices, which are generally encapsulated in another semiconductor matrix, is crucial for QD growth and device design. It is therefore essential to characterise QD structure and chemistry at the atomic scale.

Although STM has been used to achieve atomic resolution images of surface dots, it cannot be used to examine buried QD structures other than in cross-section [11]. Transmission electron microscopy (TEM) has been used widely to characterise both capped and uncapped semiconducting quantum dots using both conventional diffraction [12, 13] and phase contrast imaging, as well as spectroscopic methods such as energy-filtering TEM (EFTEM) [14, 15, 16] and energy dispersive X-ray spectroscopy (EDXS). Although many useful results have been obtained using different TEM based techniques, a clear picture of the structure of buried QDs has still not been obtained. This is due in part to the coherent nature of strained Ge/Si dots, means that phase-contrast high-resolution TEM (HRTEM) imaging does not provide sufficient contrast from Ge/Si QDs that are embedded in a Si matrix, and the insufficient spatial resolution in many spectroscopic methods.

Atomic resolution high-angle annular dark-field scanning transmission electron microscopy, termed Z-contrast imaging, is a promising and important tool for the assessment of chemical information at the atomic scale. In a Z-contrast image, the intensity is detected at high angles and over a large angular range. Each atom column is considered to scatter independently, with a cross-section approaching a Z^2 dependence (or more precisely $Z^{1.7}$) where Z is atomic number [17, 18, 19]. With care, this detection geometry yields an incoherent image in which changes in defocus and thickness do not cause contrast reversals in an atomic-resolution image. In the present work, we have studied both buried and uncapped Ge/Si quantum dots as well as their associated wetting layers, using aberration-corrected annular dark-field scanning transmission electron microscopy. Atomic resolution imaging of the interface between the Ge QDs and the surrounding Si matrix has been achieved.

EXPERIMENTAL DETAILS

The Ge/Si QD samples examined in the present study were grown by gas source molecular beam epitaxy (GSMBE), using Si_2H_6 and GeH_4 as the source gases. The pressures in the Si_2H_6 and GeH_4 source lines were fixed at 5 and 10 Torr, respectively. The structure of the sample used for this investigation is shown in Fig. 1. The growth temperature for Ge was 600°C, and the nominal Ge coverage is 5.8 ML. The spacing between adjacent QD layers is 80 nm, large enough to ignore the interaction between different layers of QDs [20], and the surface QDs can also be assumed to be unaffected by internal QDs.

Cross-sectional specimens were made by mechanical polishing, dimpling and precision ion-milling, which was performed with a low ion beam energy (2.5-3 keV) to minimize the radiation damage. Diffraction contrast TEM was performed with a JEOL 2000FX microscope, and HRTEM lattice images were recorded using JEOL 4000EX

microscope. Z-contrast ADF-STEM imaging was performed at 100kV using a dedicated STEM VG HB501 microscope equipped with a Nion spherical aberration corrector. Images were obtained using the HAADF detector with an angular range of acceptance of between 70 to 210 mrad. A schematic diagram of the STEM instrument is shown in Fig. 2. The specimen thickness used in STEM can be measured from the electron energy loss spectrum (EELS).

EXPERIMENTAL RESULTS

Firstly, the uncapped Ge QDs were investigated by high-resolution ADF-STEM imaging. Fig. 3(a) is a conventional bright-field TEM image of an area containing two uncapped QDs. No compositional information can be obtained from this image. The two dots

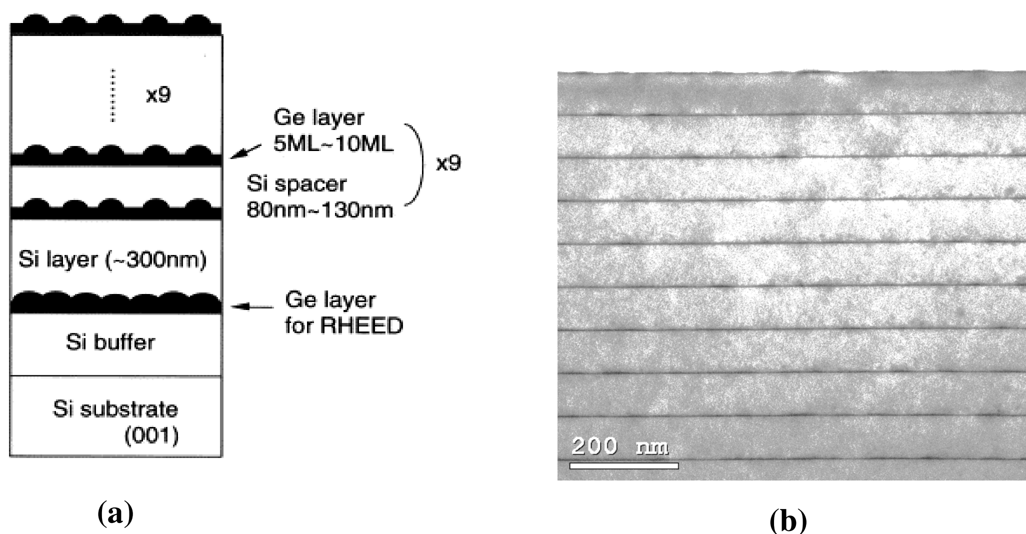

Figure 1. (a) Schematic illustration of the multilayered Ge QD sample examined in the present study. (b) Cross-sectional bright-field TEM image of the QD sample.

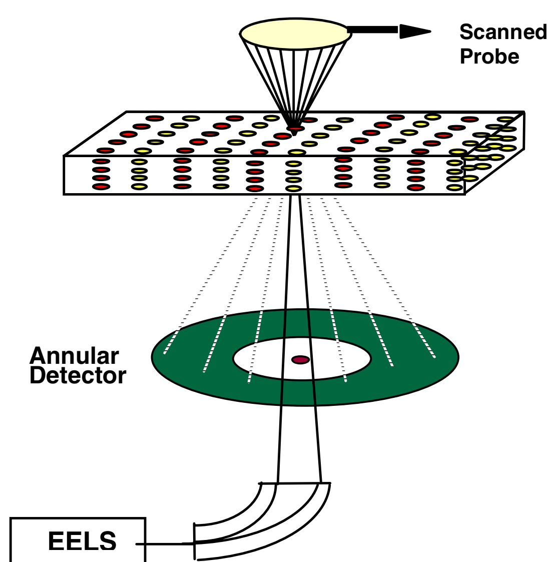

Figure 2. Schematic diagram of imaging in a STEM instrument.

are both {105}-facetted, with an 8° angle, which corresponds to the angle caused by {105} facet projection onto (110) plane, can be measured between QD edge and substrate (001) plane. Both uncapped Ge QDs were clearly distinguished by Z-contrast STEM imaging along <110>, as shown in Fig. 3(b). The Z-contrast STEM image was colorized according to intensity in order to better visualize the composition profile within and nearby a Ge QD. An intensity profile across the centre of the Ge QD is shown in Fig. 3(c). The quantum dot/substrate interface can be identified in the line profile, and the region of depletion of Ge in the dot at its base centre is determined to be about 1 nm. The result here also shows an apparent non-uniform intensity distribution in the Ge/Si QD in Fig. 3(b) with the highest intensity at the centre of the dot. Assuming that the centre of the dot spans the thickness of the specimen in the electron beam detection, and assuming a $Z^{1.7}$ dependence of the intensity after background subtraction, the Ge content at the centre of the dot is inferred to be close to 100% by comparing the intensity of Ge-containing column with that of the Si matrix. There is no bright contrast at the edges of the QD, which implies that there is no Ge rich wetting layer at the near-edge surface. Further Z-contrast STEM images obtained from the area between two uncapped QDs confirmed that the average Ge content in the quantum dots is much higher than in the wetting layer. Furthermore, the lateral Ge compositional profiles in both the surface wetting layer and the dots are non-uniform. In particular, a very low Ge content is present in the region near the edges of the surface QDs.

Fig. 4 shows a high-resolution Z-contrast STEM image of a buried Ge QD viewed along <110>. We can derive the shape of the dot and the composition profile within and nearby the dot using this image. In comparison to the uncapped dot shown in Fig. 3, the height of the capped dot is ~1 nm smaller, while its base size has increased by ~30 nm. This observation suggests that elemental interdiffusion during encapsulation occurs primarily laterally. The Ge content at the centre of the dot is again inferred to be close to 100% by comparing its intensity with that of the Si matrix.

As shown in another Z-contrast STEM image in Fig. 5, the buried wetting layer has a more uniform lateral Ge compositional distribution, where compared with the surface wetting layer. A line profile taken across the wetting layer, which is also shown in Fig. 5, shows that the growth front interface (the top side in Fig. 5) is less sharp than the other interface. The wetting layer is approximately 2nm in thickness and has a 3-monolayer-thick core with an inferred Ge content of ~ 60%. The wetting layer core thickness is close to the critical thickness for island formation from layer-by-layer growth [21]. The average Ge content can be inferred to be ~ 30% across all the Ge-containing layers. The results suggest that the wetting layer becomes more uniform in laterally by the lateral diffusion during encapsulation.

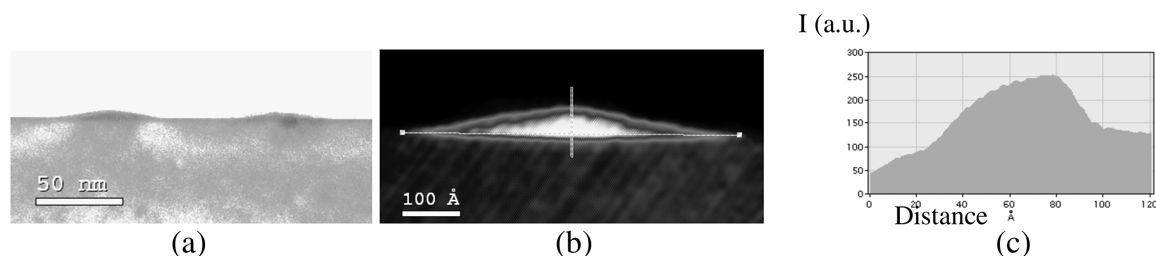

(a) (b) (c)

Figure 3. (a) Bright-field TEM image of two uncapped Ge/Si QD. (b) Z-contrast STEM image of an uncapped Ge QD. (c) Intensity profile taken along the centre of the dot.

Figure 4. Z-contrast STEM image of a buried Ge QD.

CONCLUSIONS

We have applied atomic-resolution Z-contrast imaging to investigate both uncapped and embedded Ge QDs and some outstanding features have been observed for the first time. When Ge QD forms on the Si (100) surface, there is a Si-rich zone in wetting layer surrounding the uncapped QD due to the segregation of Ge by lateral transportation from the wetting layer. During the encapsulation, the Ge content at the centre of the QD unchanged, despite significant intermixing, lateral spreading, and lateral compositional inhomogeneity inside the QD. A non-uniform wetting layer in an uncapped QD sample becomes more uniform after encapsulation. Eventually, a 3-monolayer-thick core with an inferred Ge content of ~ 60% is formed in the ~2 nm-thick wetting layer.

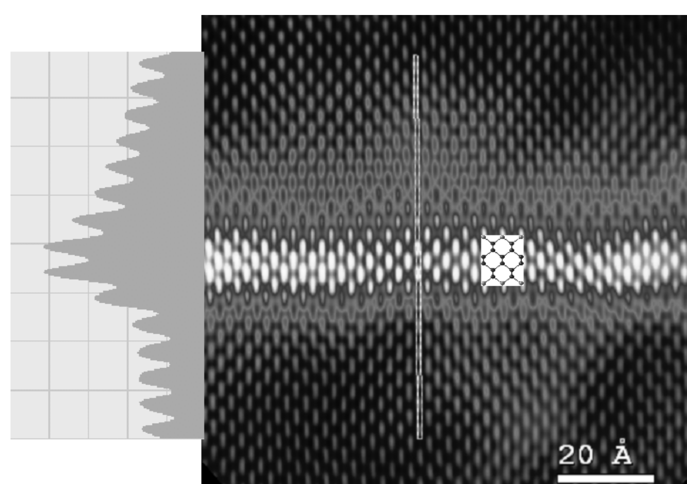

Figure 5. Z-contrast STEM image of the buried wetting layer and a profile formed from this image along the marked line.

ACKNOWLEDGMENTS

The authors thank Dr. M. Miura and Professor Y. Shiraki for MBE growth of the samples. The EPSRC and the Royal Society are thanked for financial support.

REFERENCES

1. Y. –W. Mo, D. E. Savage, B. S. Swartzentruber, M. G. Lagally, *Phys. Rev. Lett.* **65**, 1020 (1990).
2. T. I. Kamins, E. C. Carr, R. S. Williams, S. J. Rosner, *J. Appl. Phys.* **81**, 211 (1997).
3. G. Medeiros-Ribeiro, A. M. Bratkovski, T. I. Kamins, D. A. A. Ohlberg, R. S Williams, *Science* **279**,353 (1998).
4. F. M. Ross, R. M. Tromp, M. C. Reuter, *Science* **286**, 1931 (1999).
5. O. G. Schmidt, K. Eberl, *Phys. Rev. B* **61**, 13721 (2000).
6. A. Vailionis, B. Cho, G. Glass, P. Desjardins, D. G. Cahill, J. E. Greene, *Phys. Rev. Lett.* **85**, 3672 (2000).
7. D. J. H. Cockayne, X. Z. Liao, J. Zou, *Inst. Phys. Conf. Ser.* **169**, 77 (2001).
8. J. Tersoff, *Phys. Rev. Lett.* **81**, 3183 (1998).
9. J. Tersoff, B. J. Spencer, A. Rastelli, H. von Känel, *Phys. Rev. Lett.* **89**, 196104-1 (2002).
10. C. Lang, D. Nguyen-Manh, D. J. H. Cockayne, *J. Appl. Phys*. **94**, 7067 (2003).
11. D. M. Bruls, P. M. Koenraad, H. W. M. Salemink, J. H. Wolter, M. Hopkinson, M. S. Skolnick, *Appl. Phys. Lett.* **82**, 3758 (2003).
12. X. Z. Liao, J. Zou, X. F. Duan, D. J. H. Cockayne, R. Leon, C. Lobo, *Phys. Rev. B* **58**, R4235 (1998).
13. X. Z. Liao, J. Zou, X. F. Duan, D. J. H. Cockayne, Z. M. Jiang, X. Wang, *J. Appl. Phys.* **90**, 2725 (2001).
14. X. Z. Liao, J. Zou, D. J. H. Cockayne, J. Wan, Z. M. Jiang, G. Jin, K. L. Wang, *Phys. Rev. B*. **65**, 153306-1 (2002).
15. T. Walther, A. G. Cullis, D. J. Norris, M. Hopkinson, *Phys. Rev. Lett*. **86**, 2381 (2001).
16. M. Floyd, Y. Zhang, K. P. Driver, J. Drucker, P. A. Crozier, *Appl. Phys. Lett*. **82**, 1473 (2003).
17. S. J. Pennycook, D. E. Jesson, *Phys. Rev. Lett*. **64**, 938 (1990).
18. D. E. Jesson , S. J. Pennycook, J. –M. Baribeau, *Phys. Rev. Lett*. **66**, 750 (1991).
19. P. D. Nellist, S. J. Pennycook, *Ultramicroscopy* **78**, 111 (1999).
20. O. G. Schmidt, N. Y. Jin-Philipp, C. Lange, U. Denker, K. Eberl, R. Schreiner, H. Grabeldinger, H. Schweizer, *Appl. Phys. Lett.* **77**, 4138.
21. D. J. Eaglesham, M. Cerullo, *Phys. Rev. Lett*. **64**, 1943 (1990).